JACS
JOURNAL OF THE AMERICAN CHEMICAL SOCIETY
Communication
pubs.acs.org/JACS

High-Density Chemical Intercalation of Zero-Valent Copper into Bi_2Se_3 Nanoribbons

Kristie J. Koski,[†] Judy J. Cha,[†] Bryan W. Reed,[‡] Colin D. Wessells,[†] Desheng Kong,[†] and Yi Cui*[,†,§]

[†]Department of Materials Science and Engineering, Stanford University, Stanford, California 94305, United States

[‡]Physical and Life Sciences Directorate, Lawrence Livermore National Laboratory, 7000 East Avenue, Livermore, California 94550, United States

[§]Stanford Institute for Materials & Energy Science, SLAC National Accelerator Laboratory, 2575 Sand Hill Road, Menlo Park, California 94025, United States

Supporting Information

ABSTRACT: A major goal of intercalation chemistry is to intercalate high densities of guest species without disrupting the host lattice. Many intercalant concentrations, however, are limited by the charge of the guest species. Here we have developed a general solution-based chemical method for intercalating extraordinarily high densities of zero-valent copper metal into layered Bi_2Se_3 nanoribbons. Up to 60 atom % copper ($Cu_{7.5}Bi_2Se_3$) can be intercalated with no disruption to the host lattice using a solution disproportionation redox reaction.

Layered 2D nanomaterials have attracted much recent research interest because of their unique crystal and electronic structures and associated size effects.[1−6] Particularly important in layered materials is the ability to insert molecules, ions, and atoms between the layers. A hot field for many previous decades, intercalation chemistry has recently enjoyed renewed interest driven by the need for new energy storage materials,[7−14] the creation of atomically thin materials for electronic applications,[1] and tuning of the physical nature of exotic materials such as converting topological insulators to superconductors.[15−17]

Tuning the intercalant concentration yields many surprising and unusual physical and chemical phenomena, including charge density waves, anisotropic transport properties, spontaneous magnetization, two-dimensional (2D) electron-gas physics, and superconductivity.[8,9,18−20] Though intercalation of alkali metals such as lithium[10] can be high because of their small size, most intercalation concentrations are limited by the ionic nature of the intercalant.[7−10] The predominantly ionic nature of a guest species requires either a change in the host lattice oxidation states or the presence of atomic vacancies to maintain charge neutrality, thus limiting the intercalant concentration.[10] A zero-valent intercalant does not require a change in the oxidation state of the host lattice, thus allowing a high intercalation concentration.[21−26] Experimentally, successful superstoichiometric intercalation of neutral atoms has been limited to the unique case of mercury intercalation into transition-metal dichalcogenides (e.g., Hg_xTiS_2, $0 \leq x \leq 1.25$).[21−26] In this type of reaction, mercury is typically intercalated into a dichalcogenide by heating stoichiometric ratios of the materials at high temperature.

In this work, we have developed a chemical strategy for intercalating superstoichiometric amounts of copper into layered Bi_2Se_3 nanoribbons, a material recently discovered as a topological insulator,[27,28] using a low-temperature solution disproportionation redox reaction. Previous strategies for intercalating copper into Bi_2Se_3 have employed either heating stoichiometric amounts of copper, bismuth, and selenium[15−17] or electrochemical insertion using copper iodide in acetonitrile.[29] These strategies have not yielded concentrations above ∼3 atom % Cu (i.e., $Cu_{0.15}Bi_2Se_3$),[15−17,27] likely because the intercalated copper is in the +1 oxidation state, which limits the maximum intercalant concentration.[7,9,10,30] Because of the zero-valent nature of copper in our reaction, our method produces up to 60 atom % copper intercalation into Bi_2Se_3 ($Cu_{7.5}Bi_2Se_3$).

Bi_2Se_3 possesses a rhombohedral structure [space group D_{3d}^5 ($R\bar{3}m$)]. Shifted hexagonal planes of bismuth and selenium stack along the c axis and repeat every five layers as Se(1)−Bi−Se(2)−Bi−Se(1), with van der Waals forces holding together neighboring Se layers (see Figure 2a). As a rigid host lattice, Bi_2Se_3 has excess space to accommodate smaller guest atoms in the van der Waals gaps and in interstitial sites.[5] Bi_2Se_3 nanoribbons were grown using the vapor−liquid−solid (VLS) method of ref 31 using quartz growth substrates rather than silicon substrates. Yields were on the order of 5 ± 3 mg per process run. Nanoribbons grown by this method tend to have sharp edges and exceptionally high crystallinity, which enable maximum intercalation. Nanoribbons were 50 nm thick on average, with widths and lengths ranging from hundreds of nanometers to several micrometers.

It is well-known[32] that monovalent copper tends to disproportionate in solution according to the equation

$$2Cu^+(aq) \rightleftarrows Cu^0 + Cu^{2+}(aq)$$

The resulting Cu^{2+} is bound in a solvent complex, thus leaving free Cu^0 dilute in solution.[33,34] Zero-valent copper atoms were intercalated through the disproportionation redox reaction of an air-stable Cu^+ salt, tetrakis(acetonitrile)copper(I) hexafluorophosphate (Sigma-Aldrich), in acetone. In a typical reaction, the nanoribbons on the quartz substrate were placed into a solution of the salt and solvent, heated to just below reflux, for

Received: January 12, 2012
Published: April 23, 2012

   dx.doi.org/10.1021/ja300368x | J. Am. Chem. Soc. 2012, 134, 7584−7587

varying amounts of time. Care was taken to control the initial pH of the glassware, which was cleaned in an acid or base bath, kept overnight in distilled water to neutralize it, and then fully dried before use. The initial pH of the salt solution was 5−6.5. The substrates were then removed from the solution mixture and rinsed with hot acetone and hot ethanol (∼45 °C). After intercalation, no copper precipitates or particles were observed with transmission electron microscopy (TEM), with scanning TEM (STEM), or in electron diffraction or X-ray diffraction (XRD) patterns.

Several different characterization techniques were used to determine the elemental composition, structure, lattice constants, and oxidation states of the intercalant. In-situ TEM diffraction and images were acquired on a FEI Tecnai G2 F20 electron microscope at 200 keV with a Gatan double-tilt heating holder. Electron energy loss spectroscopy (EELS) was performed using a FEI Titan 80−300 instrument at 300 keV. XRD data were acquired with a PANalytical X'Pert diffractometer using copper K-edge (1.54 Å) X-rays. Rietveld refinement was used to determine the Bi_2Se_3 lattice constants. X-ray photoelectron spectroscopy (XPS) data was performed with a PHI VersaProbe Scanning XPS Microprobe using Al Kα radiation (1486 eV). Ribbons were transferred to a silicon substrate for XPS measurements. Electrical transport properties of nanoribbon devices fabricated by standard electron-beam lithography with thermally evaporated Cr/Au contacts were measured with a four-point probe method using a digital lock-in amplifier (Stanford Research Systems SR830). Atomic structures were visualized using jmol.[35]

The intercalant amount was determined by energy-dispersive X-ray spectroscopy (EDX) with a sensitivity of 1−2 atom % on single nanoribbons. The left panel of Figure 1 presents a sample

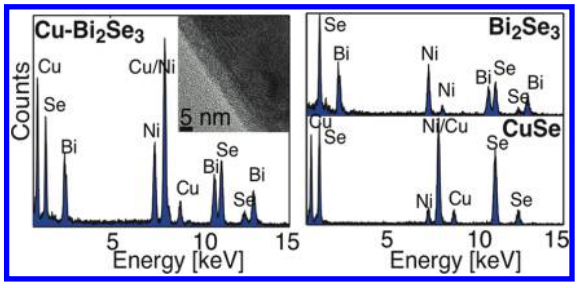

Figure 1. (left) EDX spectrum of a Bi_2Se_3 nanoribbon intercalated with 40 atom % copper, showing the high percentage of copper intercalant. The TEM image (inset) shows that no copper precipitates were present. (top right) The control spectrum of Bi_2Se_3 nanoribbons clearly demonstrates that the Bi:Se ratio did not change upon Cu intercalation. (bottom right) The EDX spectrum of CuSe, which contains 50 atom % copper, shows that a significant amount of copper was intercalated into the nanoribbon. A nickel TEM grid with a carbon support was used.

EDX spectrum from a nanoribbon intercalated with 40 atom % copper; a TEM image is shown in the inset. The control spectrum of a Bi_2Se_3 nanoribbon (Figure 1, top right) demonstrates that the ratios of bismuth to selenium did not change when copper was intercalated to high concentrations, showing that no cation exchange of bismuth with copper occurred. The large amounts of intercalated copper were demonstrated by a comparison to the EDX spectrum of copper(II) selenide obtained from Fisher Scientific (Figure 1, bottom right), in which the copper concentration should be 50 atom %.

The intercalated concentration of copper can be controlled by varying the reaction time (Figure 2b, top) or the salt

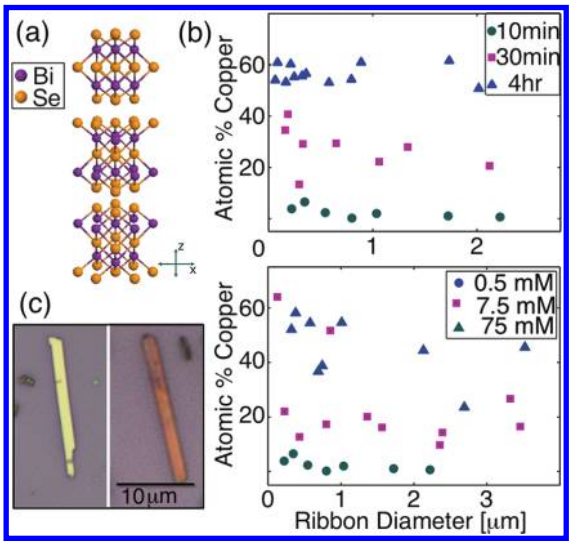

Figure 2. (a) Bi_2Se_3 is a layered chalcogenide material with a rhombohedral crystal structure. (b) High densities of copper can be chemically intercalated into Bi_2Se_3 nanoribbons using a disproportionation redox reaction with a Cu^+ salt. The amount of copper could be controlled by varying the reaction time (top) or the reactant concentration (bottom), as measured using EDX on single nanoribbons in TEM. There was no dependence of the intercalant concentration on the ribbon width. (c) Optical micrographs of Bi_2Se_3 (right) with and (left) without high-density Cu intercalation, showing a change in color to a reddish hue upon intercalation.

concentration (Figure 2b, bottom). For example, refluxing the ribbons in a solution with a Cu^+ salt concentration of 0.5 mM for 10 min intercalated less than 10 atom % copper into the ribbons; at 7.5 mM Cu^+ for 10 min, 20−30 atom % copper was intercalated, and at a high concentration of 75 mM Cu^+ for 10 min, up to 60 atom % copper was intercalated ($Cu_{7.5}Bi_2Se_3$). Variation of the nanoribbon width up to several micrometers (Figure 2b) had no impact on the amount of intercalated copper. High copper concentrations of ∼50 atom % were confirmed by bulk ensemble compositional analysis using XPS (Figure 3a), whereas EDX analysis of single ribbons showed consistent concentrations of copper in the range 45−60 atom %.

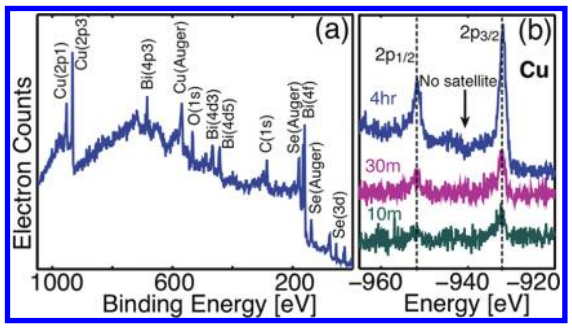

Figure 3. XPS on an ensemble of nanoribbons (a) confirms high concentrations (50%) of intercalated copper at long reaction times and (b) shows no satellite peaks, which are evidence of Cu^{2+}, confirming the absence of Cu^{2+}.[36,37]

dx.doi.org/10.1021/ja300368x | J. Am. Chem. Soc. 2012, 134, 7584−7587

The zero-valent oxidation state of the ultrahigh concentrations of Cu in the nanoribbons was confirmed by the following careful studies. First, we used EELS fine structure; EELS is a powerful technique for identifying the oxidation states of a transition metal on the basis of the near-edge fine structure, such as the L_3/L_2 ratio.[36] The fine structure of copper in nonzero oxidation states, such as Cu^+ or Cu^{2+}, shows distinct, intense, sharp L_2 and L_3 edges, whereas Cu^0 shows only broad edges (characteristic spectra are shown in Figure 4).[37] EELS spectra of individual Cu-intercalated Bi_2Se_3 nanoribbons revealed that the intercalated copper was in the zero oxidation state (Cu^0) (Figure 4).

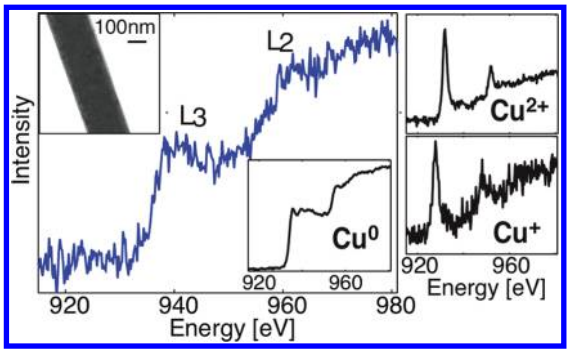

Figure 4. (left) EELS fine structure reveals that the copper intercalated in the Bi_2Se_3 nanoribbons is zero-valent. Insets: (top left) TEM image of the nanoribbon; (bottom right) EELS spectrum of Cu^0 from a 30 nm thermally evaporated Cu metal film on a Ni TEM grid. (right) Reference EELS spectra for (top) Cu^{2+} from CuSe powder and (bottom) Cu^+ from the powdered precursor salt tetrakis(acetonitrile)-copper(I) hexafluorophosphate.

A second method used to determine the oxidation state of the copper in the ribbon was XPS. When the oxidation state of copper is Cu^{2+}, XPS shows distinct satellite peaks.[38,39] However, the XPS spectrum of an ensemble of intercalated nanoribbons (Figure 3b) showed no satellite peaks characteristic of Cu^{2+} ions. Third, single-nanoribbon electrical devices were fabricated to compare the conductivities before and after Cu intercalation. Typical sheet resistances of copper-intercalated Bi_2Se_3 (10–60 atom % intercalant) were measured to be $26 \pm 2\ \Omega/\square$ at room temperature with a typical thickness of ~50 nm, corresponding to a resistivity of $\sim 1.3 \times 10^{-4}\ \Omega$ cm. Without Cu, typical sheet resistances of Bi_2Se_3 were 200–300 $\Omega/\square$, corresponding to a resistivity of $(1-1.5) \times 10^{-3}\ \Omega$ cm. The intercalation of zero-valent metallic copper would be expected to enhance the total conductivity significantly (the resistivity of copper is $\sim 1.7 \times 10^{-6}\ \Omega$ cm). Finally, an optical microscopy image of the Cu-intercalated nanoribbons appeared reddish, close to the color of Cu metal (Figure 2c), suggesting high concentrations of zero-valent copper. The reddish color was observed in all of the Cu-intercalated Bi_2Se_3 nanoribbons independent of lateral width or vertical thickness, confirming the reddish color to be an intrinsic property and not merely an interference effect. This reddish color could not be explained by the possible formation of Cu(I) or Cu(II) compounds such as Cu_2Se and CuSe (which look black because of their small band gaps) or CuO (which should appear blue). The zero-valent nature of the copper intercalant allows superstoichiometric intercalation concentrations in Bi_2Se_3.

Single-crystal superlattice patterns observed with electron diffraction are a signature of intercalation.[7−9] In pristine Bi_2Se_3 nanoribbons or nanoribbons with a Cu concentration below 10 atom %, electron diffraction gave the regular Bi_2Se_3 [001] hexagonal pattern without any additional detectable diffraction spots (Figure 5a, right). Above 10% copper intercalation,

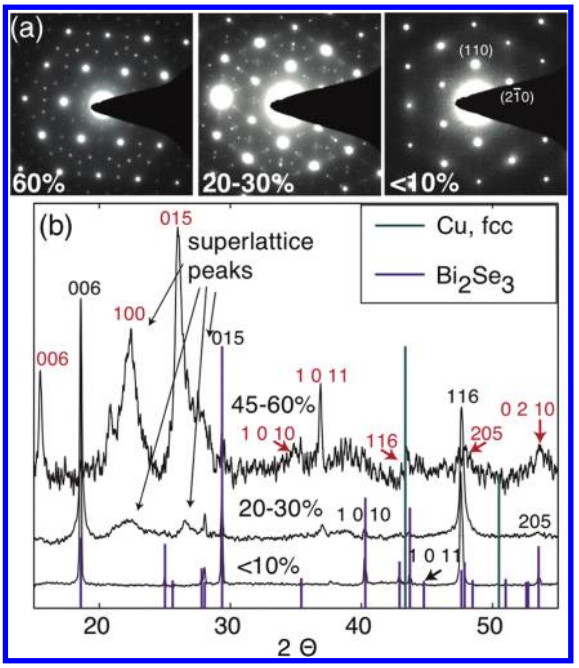

Figure 5. (a) Representative electron diffraction patterns demonstrate the wide variety of superlattice patterns observed upon intercalation. (b) XRD patterns of Cu-intercalated Bi_2Se_3 show a large lattice expansion of the host crystal to accommodate high densities of copper. Values of *hkl* are shown in purple for lower concentrations of copper intercalant and red for higher. No fcc copper was seen, confirming the absence of copper precipitates.

enough copper atoms occupy the host lattice to become ordered and form superlattice spots in the electron diffraction pattern (Figure 5a, left and middle). The electron diffraction patterns of Cu-intercalated Bi_2Se_3 showed no polycrystalline rings corresponding to face-centered cubic (fcc) copper, confirming that no Cu precipitated on the nanoribbon surface. At the highest intercalation densities in nanoribbons (60 atom %), a characteristic superlattice pattern is formed in which a hexagon of 12 superlattice spots surrounds each of the host lattice spots (Figure 5a, left). This superlattice pattern is similar to that of Na intercalated in TiS_2.[8]

The high density of copper intercalation was further confirmed by an increase in lattice spacing along both the *a* and *c* axes. Lattice expansion is considered to be evidence of intercalation[40] and was detected with XRD of Cu-intercalated Bi_2Se_3 with increasing copper intercalant (Figure 5b). Superlattice peaks, indicated with arrows, were identified in the XRD patterns, consistent with the spot positions in the electron diffraction patterns. Again, no fcc copper was seen, consistent with the absence of copper metal precipitates. Rietveld refinement of the Bi_2Se_3 host lattice structure with no copper determined that $a = 4.14 \pm 0.01$ Å and $c = 28.5 \pm 0.01$ Å. For Cu-intercalated Bi_2Se_3, the value of *a* ranged from 4.14 ± 0.01 Å for <10 atom % Cu to 4.54 ± 0.74 Å at maximum intercalation. Electron diffraction confirmed that $a = 4.5$ Å for a single ribbon intercalated with 60% copper. The *c* lattice constant noticeably increased to 28.6 ± 0.01 Å for <10 atom % Cu and 34.1 ± 0.76 Å for 60 atom % Cu. Therefore, the *c*

dx.doi.org/10.1021/ja300368x | J. Am. Chem. Soc. 2012, 134, 7584−7587

direction expands dramatically upon full intercalation (~21%). From Rietveld refinement, the average crystallite sizes were 3.2 μm for samples with <10 atom % Cu and 3.2 μm for samples with 45−60% Cu. To attain such a high concentration, copper may occupy not only the van der Waals gaps but also the interstitial sites of each layer, or it may exist as biatomic or triatomic layers in the van der Waals gaps.

Intercalation of copper into layered chalcogenide materials at such high concentrations has not been observed previously.[7,9,10] We suspect that the high crystal quality and sharp edges of the VLS-grown nanoribbons combined with the low-temperature, noninvasive chemical treatment enhanced the intercalation concentration. TEM images and electron diffraction patterns (Figure 1, inset; Figure 4, inset; Figure 5a) showed that the Cu-intercalated nanoribbons are single crystals with low defect densities and sharp edges, with the crystallographic *c* axis normal to the top and bottom surfaces. A likely path for introducing copper is through the sharp edges of the crystalline ribbons. TEM images showed that the low-temperature synthesis conditions leave the ribbons relatively unperturbed.

This investigation offers a new method for intercalating extraordinarily high densities of zero-valent copper atoms into Bi_2Se_3 nanoribbons without disrupting the host lattice. In ongoing investigations, we have found that this method is general and that high densities of copper can be intercalated into other layered materials such as In_2Se_3 and GaSe. Similar reactions may be used to intercalate a variety of other zero-valent metallic atoms into Bi_2Se_3 and many other layered materials. We foresee an enormous potential impact of this methodology in establishing fundamentally new and unexpected physical behaviors.

■ ASSOCIATED CONTENT

Ⓢ Supporting Information

High-resolution TEM image of 60 atom % Cu-intercalated Bi_2Se_3 and complete ref 1. This material is available free of charge via the Internet at http://pubs.acs.org.

■ AUTHOR INFORMATION

Corresponding Author

yicui@stanford.edu

Notes

The authors declare no competing financial interest.

■ ACKNOWLEDGMENTS

Y.C. acknowledges support from a King Abdullah University of Science and Technology (KAUST) Investigator Award (KUS-l1-001-12), the Keck Foundation, and the DARPA MESO Project (N66001-11-1-4105). B.W.R. was supported through grants from the U.S. Department of Energy (DOE), Office of Basic Energy Sciences, Division of Materials Science and Engineering, and the work was performed under the auspices of DOE by LLNL under Contract DE-AC52-07NA27344.

■ REFERENCES

(1) Coleman, J. N.; et al. *Science* **2011**, *331*, 568.
(2) Tenne, R. *Nat. Nanotechnol.* **2006**, *1*, 103.
(3) Seo, J.-W.; Jun, Y.-W.; Park, S.-W.; Nah, H.; Moon, T.; Park, B.; Kim, J.-G.; Kim, Y. J.; Cheon, J. *Angew.Chem.,Int. Ed.* **2007**, *46*, 8828.
(4) Geim, A. K. *Science* **2009**, *324*, 1530.
(5) Zhang, Y.; Tan, Y.; Stormer, H. L.; Kim, P. *Nature* **2005**, *438*, 201.
(6) Peng, H.; Schoen, D. T.; Meister, S.; Zhang, X. F.; Cui, Y. *J. Am. Chem. Soc.* **2007**, *129*, 34.
(7) *Progress in Intercalation Research*; Müller-Warmuth, W., Schöllhorn, R., Eds.; Kluwer: Dordrecht, The Netherlands, 1994.
(8) *Intercalation in Layered Materials*; Dresselhaus, M. S., Ed.; NATO ASI Series, Subseries B, Physics, Vol. *148*; Plenum Press: New York, 1987.
(9) *Intercalated Layered Materials*; Levy, F., Ed.; Reidel: Dordrecht, The Netherlands, 1979.
(10) *Intercalation Chemistry*; Whittingham, M. S., Jacobson, A. J., Eds.; Academic Press: New York, 1982.
(11) Whittingham, M. S. *J. Solid State Chem.* **1979**, *29*, 303.
(12) Aricò, A. S.; Bruce, P.; Scrosati, B.; Tarascon, J.-M.; Schalkwijk, W. V. *Nat. Mater.* **2005**, *4*, 366.
(13) Kang, K.; Meng, Y. S.; Breger, J.; Grey, C. P.; Ceder, G. *Science* **2006**, *311*, 977.
(14) Tarascon, J.-M.; Armand, M. *Nature* **2008**, *451*, 652.
(15) Hor, Y. S.; Williams, A. J.; Checkelsky, J. G.; Roushan, P.; Seo, J.; Xu, Q.; Zandbergen, H. W.; Yazdani, A.; Ong, N. P.; Cava, R. J. *Phys. Rev. Lett.* **2010**, *104*, No. 057001.
(16) Hor, Y. S.; Checkelsky, J. G.; Qu, D.; Ong, N. P.; Cava, R. J. *J. Phys. Chem. Solids* **2011**, *72*, 572.
(17) Wray, L. A.; Xu, S.-Y; Xia, Y.; Hor, Y. S.; Qian, D.; Fedorov, A. V.; Lin, H.; Bansil, A.; Cava, R. J.; Hasan, M. Z. *Nat. Phys.* **2010**, *6*, 855.
(18) Gamble, F. R.; DiSalvo, F. J.; Klemm, R. A.; Geballe, T. H. *Science* **1970**, *168*, 568.
(19) Morosan, E.; Zandbergen, H. W.; Dennis, B. S.; Bos, W. G.; Onose, Y.; Klimczuk, T.; Ramirez, A. P.; Ong, N. P.; Cava, R. J. *Nat. Phys.* **2006**, *2*, 544.
(20) Weller, T. E.; Ellerby, M.; Saxena, S. S.; Smith, R. P.; Skipper, N. T. *Nat. Phys.* **2005**, *1*, 39.
(21) Ganal, P.; Moreau, P.; Ouvrard, G.; Sidorov, M.; McKelvy, M.; Glaunsinger, W. *Chem. Mater.* **1995**, *7*, 1132.
(22) Sidorov, M.; McKelvy, M.; Sharma, R.; Glaunsinger, W.; Ganal, P.; Moreau, P.; Ouvrard, G. *Chem. Mater.* **1995**, *7*, 1140.
(23) Sidorov, M. V.; McKelvy, M. J.; Sharma, R.; Glaunsinger, W. S. *J. Solid State Chem.* **1998**, *141*, 330.
(24) Sidorov, M. V.; McKelvy, M. J.; Cowley, J. M.; Glaunsinger, W. S. *Chem. Mater.* **1998**, *10*, 3290.
(25) McKelvy, M. J.; Sharma, R.; Glaunsinger, W. S. *Chem. Mater.* **1991**, *3*, 783.
(26) McKelvy, M. J.; Sharma, R.; Glaunsinger, W. S. *Solid State Ionics* **1993**, *63−65*, 369.
(27) Zhang, H.; Liu, C.-X.; Zi, X.-L.; Dai, X.; Fang, Z.; Zahng, S.-C. *Nat. Phys.* **2009**, *5*, 438.
(28) Peng, H.; Lai, K.; Kong, D.; Meister, S.; Chen, Y.; Zi, X.-L.; Zhang, S.-C.; Shen, Z.-X.; Cui, Y. *Nat. Mater.* **2010**, *9*, 225.
(29) Kriener, M.; Segawa, K.; Ren, Z.; Sasaki, S.; Ando, Y. *Phys. Rev. Lett.* **2011**, *106*, No. 127004.
(30) Vaško, A.; Tichý, L.; Horák, J.; Weissenstein, J. *Appl. Phys. A: Mater. Sci. Process.* **1974**, *5*, 217.
(31) Kong, D.; Dang, W.; Cha, J. J.; Li, H.; Meister, S.; Peng, H.; Liu, Z.; Cui, Y. *Nano Lett.* **2010**, *10*, 2245.
(32) MacKay, K. M. *Introduction to Modern Inorganic Chemistry*, 6th ed.; CRC Press: Boca Raton, FL, 2002.
(33) Rosen, B. M.; Jiang, X.; Wilson, C. J.; Nguyen, N. H.; Monteiro, M. J.; Percec, V. *J. Polym. Sci., Part A: Polym. Chem.* **2009**, *47*, 5606.
(34) Coetzee, J. F.; Siao, W. S. *Inorg. Chem.* **1963**, *2*, 14.
(35) http://www.jmol.org.
(36) Egerton, R. F. *Rep. Prog. Phys.* **2009**, *72*, No. 016502.
(37) Leapman, R. D.; Grunes, L. A.; Fejes, P. L. *Phys. Rev. B* **1982**, *26*, 614.
(38) Hüfner, S. *Photoelectron Spectroscopy: Principles and Applications*, 3rd ed.; Springer: Berlin, 2003; p111.
(39) Panzner, G.; Egert, B.; Schmidt, H. P. *Surf. Sci.* **1985**, *151*, 400.
(40) Powell, A. V. *Annu. Rep. Prog. Chem., Sect. C: Phys. Chem.* **1993**, *90*, 177.